DOI: 10.13009/EUCASS2023-375
Aerospace Europe Conference 2023 – 10TH EUCASS – 9TH CEAS

First order thermal analysis methodology for hybrid-electric propelled aircraft in early design stages

J. van Muijden[*†] and V.J.E. Aalbers*[*]*
** Royal Netherlands Aerospace Centre NLR*
Anthony Fokkerweg 2, 1059 CM Amsterdam, The Netherlands
Jaap.van.Muijden@nlr.nl – Jos.Aalbers@nlr.nl
[†] Corresponding Author

Abstract
This paper describes the approach undertaken within the framework of the IMOTHEP project to arrive at a useful predictive methodology for thermal analysis and design within the early design stages of commercial aircraft. The drivetrains are assumed to be of hybrid-electric nature, suitable for a SMR-type aircraft. The elaboration focuses on the lay-out of the configuration, the specifics of the drivetrain, the integration of subsystems and their thermal simulation approach, and on the impact of parameter variations on the predicted outcomes. The presented methodology provides insight into the impact of assumptions during the design phase on thermal management consequences.

1. Introduction

The growing societal demand for zero-emission transportation means and significantly greener aircraft resulting in a net-zero carbon footprint by 2050 [1] has initiated serious research into electrification options of aircraft configurations and components [2] [3] [4]. One potential possibility under scrutiny is the turboelectric configuration using a kerosene-fueled engine which drives a generator providing enough electrical energy to operate and propel the aircraft. However, this approach leads to unprecedented amounts of electric power distributed through the aircraft. Even though the efficiencies of components such as generator, motors, converters, etc. have efficiencies of 95% or higher, for megawatt class aircraft this still results in very large amounts of low-quality heat dissipated throughout the architecture that need to be rejected. The required magnitude of heat rejection is posing serious challenges for an efficient thermal management system.
This paper is a sequel to our previous paper [5] that identified the starting point and way forward for a thermal analysis methodology applicable in preliminary design stages using a minimal amount of aircraft data. The paper focuses on the enhancements achieved in estimating the heat distribution using a nodal approach, comprising dynamic thermal analysis over the full flight profile, updated compartment model to describe the configuration in reduced thermal model terms, and step-by-step implementation of the integration of (sub-)system interactions. Each compartment or component is assigned to be a node. Nodes are interconnected with other nodes allowing the exchange of heat. The thermal exchanges are described using straightforward mathematical relations for conduction, convection and radiation. Input for this nodal approach is a given typical flight profile describing the required thrust, altitude, and Mach number at each moment. Outputs are the power demands, heat rejection and resulting nodal temperatures over time. The method is intended to show how input parameter variations (e.g. the component efficiencies, assumed heat transfer coefficients, cooling loop characteristics) impact the heat rejection of components and thereby the required thermal management system. The reported work consists of results from investigations within the framework of the IMOTHEP project (Investigation and Maturation Of Technologies for Hybrid-Electric Propulsion) [6]. A general overview of the project objectives, research directions and progress is presented in [7].

2. Reprise of configuration

2.1 Configuration and drivetrain

The type of aircraft for this investigation is the Short-to-Medium Range conservative commercial aircraft (SMR-con in short) consisting of a classical tube-and-wing lay-out, selected out of the four different configurations that are being

DOI: 10.13009/EUCASS2023-375

investigated within the IMOTHEP project [7]. The aircraft has a seating capacity and installed power comparable to the A320neo. The drivetrain for this type of aircraft originates from the ONERA-developed Dragon configuration [8] and consists of two gas turbines, two electrical generators and rectifiers (originally, each gas turbine was anticipated to drive two generators), four distribution and four propulsion buses, and 24 electrical propulsor units (EPUs), placed within the aircraft as shown in Figure 1. Each EPU consists of an inverter and an electrical motor driving a ducted fan to accelerate the freestream air. The configuration shows a distributed electric propulsion (DEP) lay-out over the wing. The on-board energy source is kerosene, feeding the two gas turbines placed at the rear of the fuselage. The drivetrain is schematically shown in Figure 2. Distribution buses and propulsion buses are connected in a smart way to provide duplication of connections leading to a maximum chance of power supply to all EPUs. EPUs are connected to the propulsion buses in such a way that failure of one propulsion bus does not lead to massive asymmetrical propulsive force. The colour coding of EPUs on the wing in Figure 1 matches the colour coding of the propulsion buses in Figure 2, showing where the electrical power is originating.

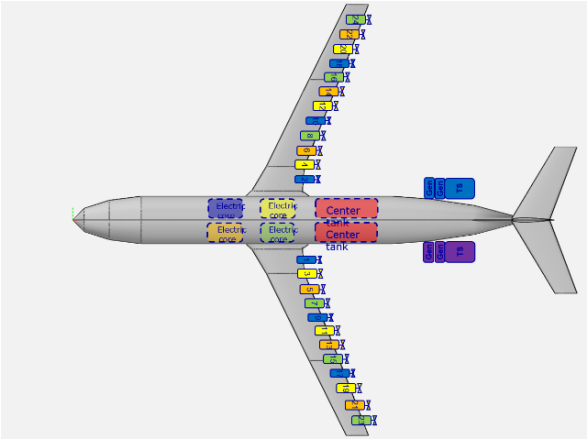

Figure 1: SMR-con configuration used for the current thermal investigations.

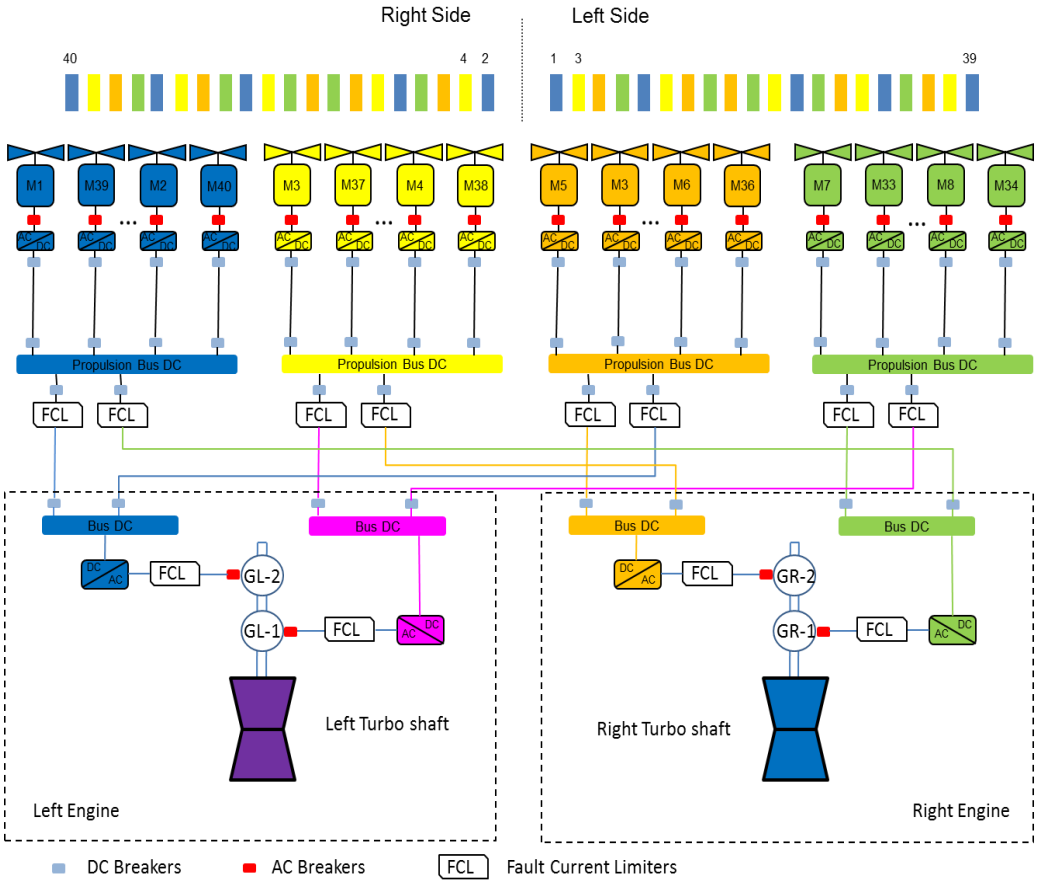

Figure 2: Schematic representation of the hybrid-electric drivetrain of the SMR-con.

DOI: 10.13009/EUCASS2023-375

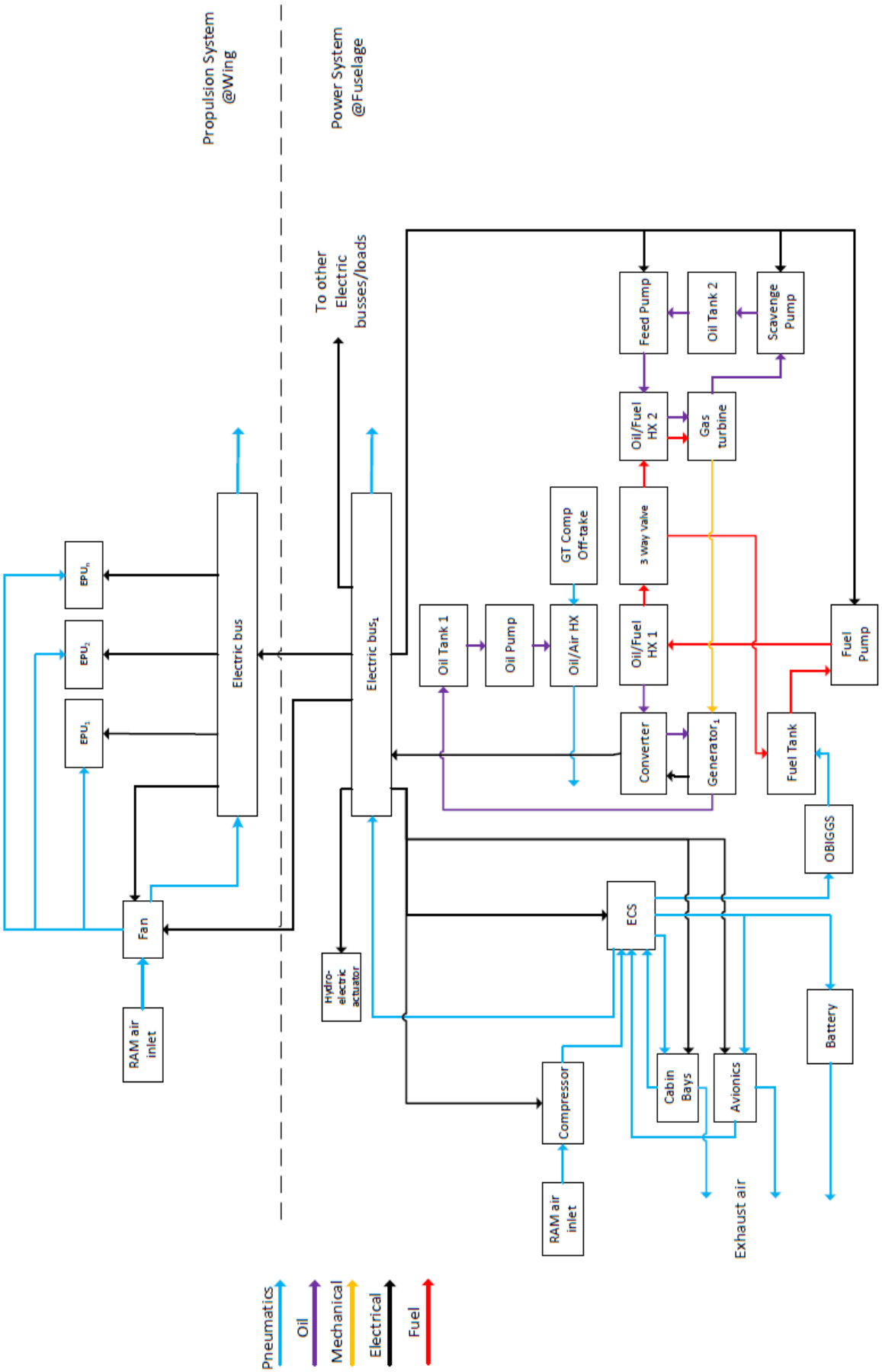

Figure 3: System interactions anticipated for the SMR-con.

DOI: 10.13009/EUCASS2023-375

Now, apart from the drivetrain components already mentioned, there are a lot of additional components involved in the interactions between systems and subsystems that make the aircraft work. The interactions between systems can be of various nature: either mechanical, electrical, pneumatic for air cooling or pressurization purposes, or fluidic for fuel and oil cooling. The thermal management system (TMS) is part of these interactions by providing cooling loops consisting of heat exchangers, fluid circuits, oil reservoirs, ram air inlets, etc. In a collaborative effort with consortium partners involved in the thermal management investigations, the schematic representation of the systems and system interactions has been devised as shown in Figure 3. The upper part of this figure above the dashed line shows the EPU part, mainly located on the wing of the aircraft. The lower part of the figure below the dashed line represents the power generation part, which comes with many challenges in terms of cooling the gas turbine and generators, and distribution of the electrical power to various clients. Some of the key questions are: What will be the weight of the resulting TMS? How will it impact the top level aircraft requirements? In what way are the cooling loops most efficiently done?

2.2. Heat loads over the flight profile

In our previous paper [5], heat loads were calculated and shown at selected isolated conditions during the flight. The current extension of the methodology takes the entire flight profile as input and delivers the component powers and heat loads over time. For the SMR-con, time-dependent input data for altitude, Mach number, and thrust were provided (as an example, flight profile altitude and Mach number are shown in Figure 4, left). Derivation of the heat loads is based on prescribed efficiencies for the drivetrain components, and on the power connections between those components. The power assessment and heat loads derivation starts at the propulsors. As the total thrust of the aircraft is given, each propulsor provides an equal part of this thrust. The input power of the electric motors, however, has to be a little higher to compensate for the internal power losses into heat. The same reasoning applies to the inverters, buses, rectifiers, generators and the gas turbines. At the end of this processing step, input and output powers of each drivetrain component are known, and simultaneously an impression of the heat loads over time is obtained from their difference as shown in Figure 4, right. Finally, the instantaneous fuel consumption of the gas turbines can be calculated based on their necessary power output, see Figure 5, left. Integration of the instantaneous fuel consumption over time provides the total amount of fuel burn as shown in Figure 5, right. The current implementation takes one second as time basis for calculations, chosen to accommodate the dynamic responses from interacting systems and associated cooling loops later on. In case the flight profile input data are given at coarser intervals, e.g. during cruise, linear interpolation is performed in the dataset to arrive at data for each second of the flight. It should be mentioned here that the heat loads and resulting fuel consumption will strongly depend on the efficiencies used for the different drivetrain components.

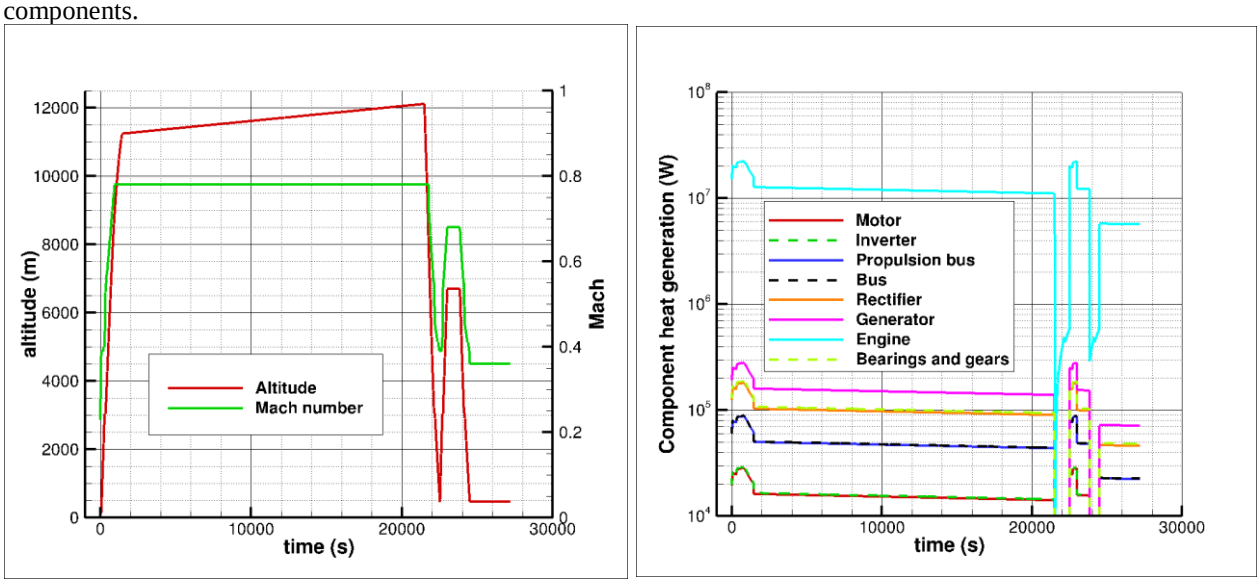

Figure 4: Example of flight profile data typical for an average flight (left), and resulting heat loads over time (right).

As reported previously [5], a set of state-of-the-art efficiencies has been assumed for these preliminary calculations. Within IMOTHEP, discussions on technological advances and projections towards the future have constantly changed the vision on component efficiencies to be used. In the current implementation of the simulator, the efficiencies of components are read from an input file and can easily be altered into more future-proof numbers. The impact of such changes will be part of the parameter variation study below.

DOI: 10.13009/EUCASS2023-375

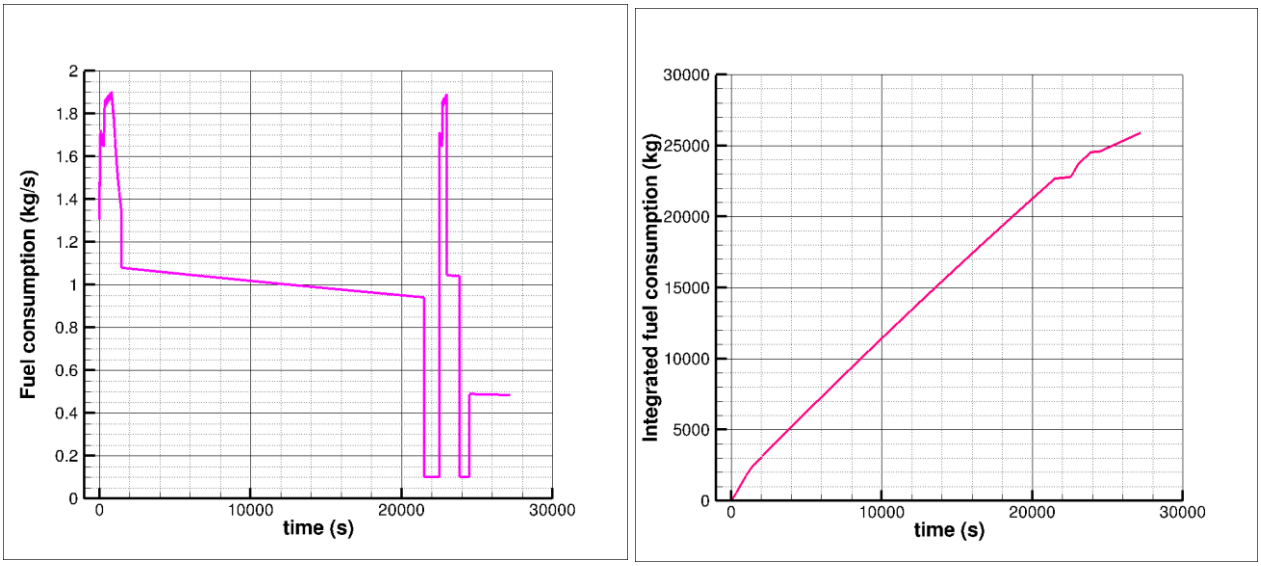

Figure 5: Instantaneous fuel consumption (left) and integrated fuel consumption over time (right).

3. Interacting system modelling

3.1 Gas turbine and generator

The most complex part of interacting systems as depicted in Figure 3 is the part around the gas turbine and generator. For the sake of clarity, a separate picture showing the main thermal control loops is given in Figure 6.

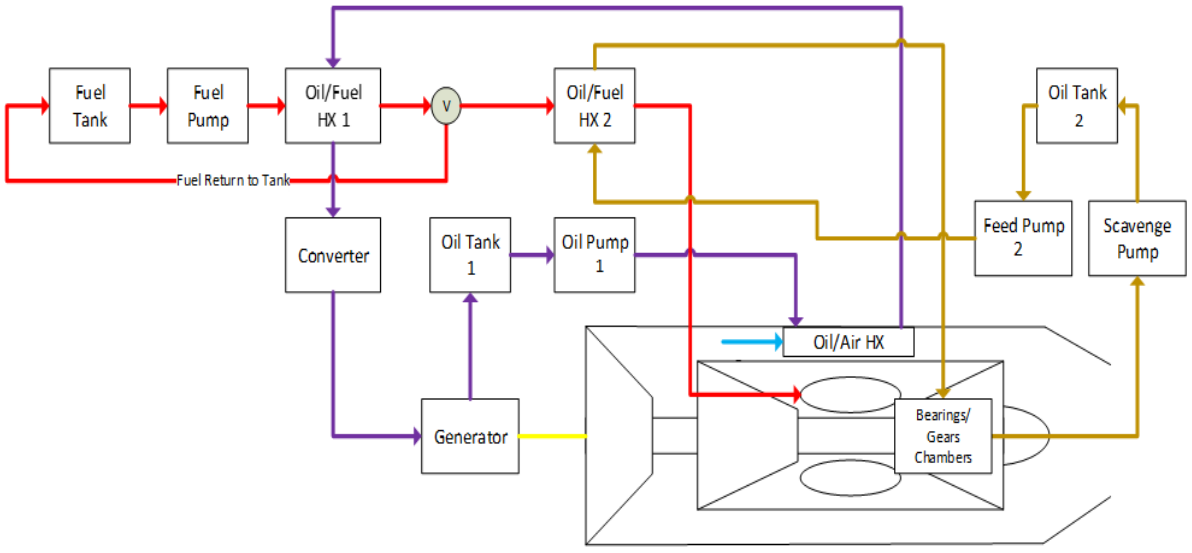

Figure 6: Thermal control of power generation part (gas turbine, generator and rectifier) of aircraft systems.

A number of different thermal control loops can be identified:

1. Beige loop in Figure 6: the gas turbine gears and bearings are lubricated and cooled with oil, provided by an oil tank and feed pump. The oil is cooled in a fuel/oil heat exchanger before being inserted into the bearings. A scavenge pump takes the oil out of the system and closes the loop in the oil tank. In the assumptions made to analyse this loop, also the mechanical generator part (bearings) is lubricated with this oil loop, indicating that part of the generator efficiency and heat are attributed to this loop.
2. Purple loop in Figure 6: the electrical part of the generator is cooled with liquid coolant which is sprayed onto the windings. The coolant comes from an oil tank, gains momentum by an oil pump and is at first cooled in an air/oil heat exchanger and in second instance in a fuel/oil heat exchanger. Before reaching the generator and flowing back into the oil tank it is first used to cool the rectifier (or inverter).

DOI: 10.13009/EUCASS2023-375

3. Red loop in Figure 6: as indicated in the above points, fuel is used as a coolant as well in order to control the temperatures of both engine oil and generator coolant. In fact, more fuel than needed for combustion is pumped up in critical flight phases (take-off, climb) to control the temperature of the generator coolant. The fuel originates from the fuel tank, the amount of fuel used for cooling and combustion is controlled by a fuel pump. At first, the fuel cools the generator coolant. In the valve following the fuel/oil heat exchanger, a (large) part of the fuel is returned to the fuel tank, depending on the flight phase. The fuel that will be combusted passes through the fuel/oil heat exchanger for cooling of the engine oil before entering the combustion chamber.
4. Blue arrow in Figure 6: the air/oil heat exchanger cools the generator coolant using ram air. Initially, the gas turbine was expected to have a minor bypass channel in which the air/oil heat exchanger could be placed. However, as the gas turbine is not expected to provide any thrust, it has been optimized for shaft power generation and the bypass was completely removed. For the air/oil heat exchanger, this implies that a separate ram air channel is needed to provide ambient air. During low-speed or no-speed conditions (start-up, taxiing, ramp waiting time), the ram air supply is insufficient or even completely lacking, therefore it was deemed necessary to extract a significant amount of bleed air from the gas turbine compressor during the low-speed conditions to provide the required momentum forcing the ram air channel flow.
5. Yellow connector in Figure 6: the shaft power needed to drive the generator is mechanically connected to the gas turbine. This mechanical connection is the reason for cooling of bearings of the generator by the engine oil loop.

For the thermal simulation of this subsystem, many assumptions from experience and best practice have been included by industrial partners. These assumptions include:

- Initial temperatures;
- Oil/coolant tank buffer volumes: these are not very large, but essential in the system modelling;
- Oil and coolant mass flows at maximum rpm;
- Amount of oil and coolant being pumped around in legacy aircraft is dependent on the rpm of the gas turbine, as pumps are mechanically coupled to the gear box connected to the shaft of the gas turbine. In future hybrid-electric aircraft, pumps are assumed to be electrical pumps as shown in Figure 3. Nevertheless, the mass flows needed to lubricate and cool the gas turbine and generator are still assumed to relate to the rpm of the gas turbine. In the current implementation within the simulator, mass flows of oil and coolant have been coupled to the requested engine power (by linking the values to the combustion fuel flow rate) due to very limited information on engine rpm. This is not an ideal situation and needs further refinement later on;
- There is a maximum temperature of lubrication oil and generator coolant in order to avoid deterioration of the fluid properties. Currently, these limits are not yet monitored by the simulator;
- Heat exchanger characteristics: in general, a heat exchanger design requires iteration and its characteristics are not a priori known. In the current version, the heat exchanger characteristics assumed by industrial partners has been adopted;
- Splitting of generator in an electrical part and a mechanical part including the associated split of the overall generator efficiency in an electrical part and a mechanical part;
- Amount of bleed air extracted from the gas turbine compressor during the low-speed conditions and the transitioning from full bleed to no bleed after several minutes in climb. Also, the temperature of the bleed air going through the air-oil heat exchanger depends on compressor stage characteristics;
- Use of the fuel-return-to-tank loop, being active only in the most thermally demanding phases of the flight. It is currently being used in take-off and climb phases;
- Fuel enhancement factor λ (note that the amount of fuel used in the first fuel-oil heat exchanger, before the return-to-tank valve, equals $(1 + \lambda)$ times the fuel that is actually used for combustion). There is a maximum temperature for the fuel in the tank, currently set at 38 ºC (311 K). There is also a maximum temperature for the fuel entering the engine, currently taken as 71.1 ºC (344.25 K). Both maximum fuel temperatures are actively being monitored by the simulator;
- The numerical values of the specific heat of oil and coolant are in general temperature dependent [9]. In the current implementation, constant values have been used although this may change as soon as convincing data have been found.

A provisional impression of the outcome of dynamic simulations for this part of the interacting systems is shown in Figure 7, pending further checks on the assumptions made and their implementation, as well as on initial conditions. The underlying mathematical equations, physical foundations and some numerical aspects of the simulator have already been explained in [5], including the international standard atmosphere (ISA) modelling and implementation of deviations from ISA.

DOI: 10.13009/EUCASS2023-375

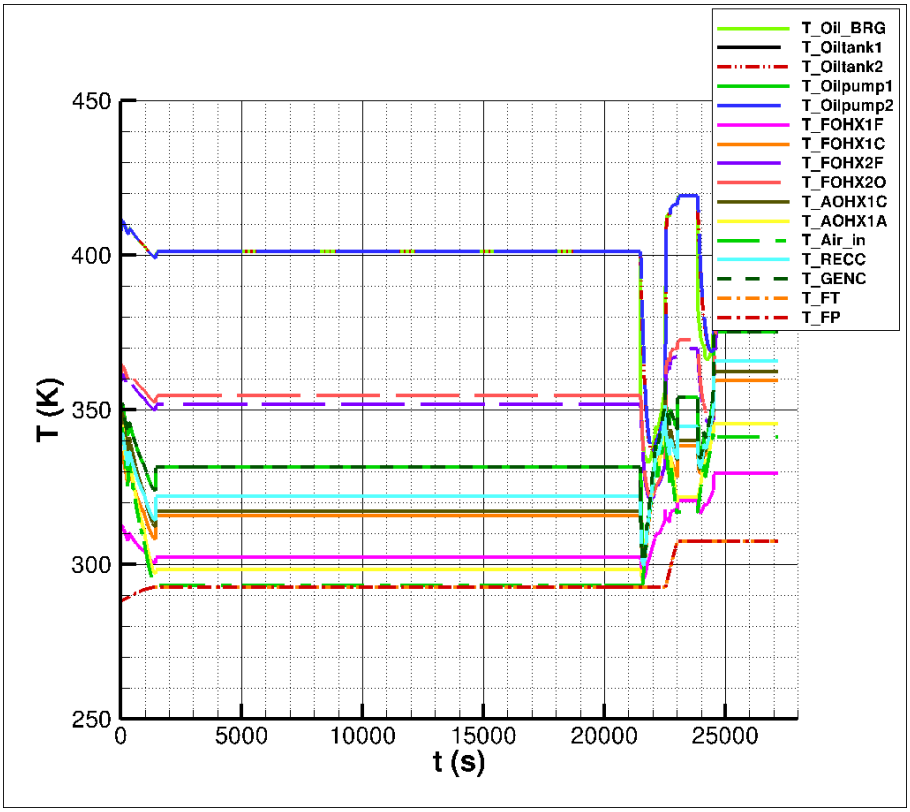

Figure 7: Dynamic simulation of temperatures of components and fluids in the power generation part.

3.2 Electrical propulsion unit

The EPU is a propulsion unit driving a ducted fan by action of an electric motor. Electric power is directed to the motor through an inverter connected to a propulsion bus. The heat generation per motor and inverter is shown in Figure 4 right. The motor and inverter, closely packed together but nevertheless regarded as separate boxes for modelling purposes, are placed in the duct such that air cooling is naturally available, see Figure 8. The air flowing through the duct is either close to freestream velocity (idle motor conditions) or at a somewhat higher velocity due to the propulsive action of the fan.

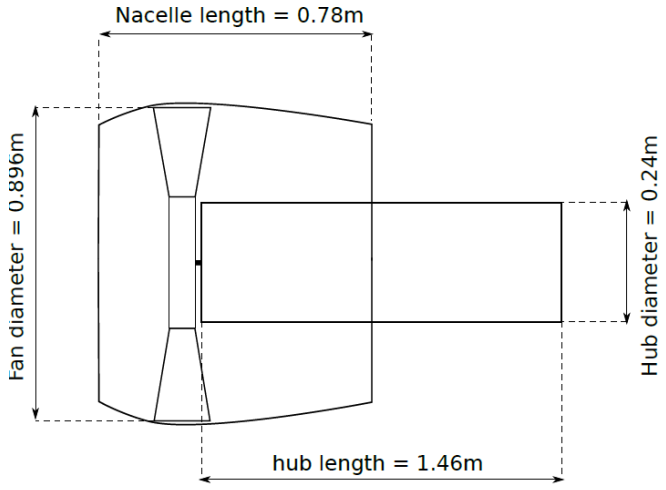

Figure 8: Schematic representation of EPU with main dimensions (picture not to scale)

For the EPU, but in similar fashion for other components, heat transfer to the air takes place by convection of the turbulent flow over the motor and inverter housing. The heat losses are calculated from convective considerations, i.e. the heat transfer coefficient is derived from relations between Nusselt and Reynolds number, details of which are given in [5]. Also, heat losses due to radiation have been included as has been elaborated in [5], although this will only play a significant role in case of high surface temperatures. For heat loss estimates, some basic geometrical dimensions of

DOI: 10.13009/EUCASS2023-375

motor and inverter are used to estimate the heat transfer area subjected to the air flowing through the duct. Currently, the heat transfer coefficient has been calculated on the basis of the length of the hub, and its value has been designated to both motor and inverter. The allocation of the hub area for motor cooling and inverter cooling can be decided based on actual dimensions; currently it is 0.75 meter of hub length for motor, and 0.71 meter of hub length for the inverter. The resulting heat rejection against the heat generation of motor and inverter, as well as provisional temperature time histories are shown in Figure 9, using the projected future efficiencies from Table 1. Heat production and heat rejection are quickly balanced as the cooling power increases with increasing surface temperature. The dynamical aspects in this balance are based on assumed heat capacities and may require further finetuning. The motor temperature is shown to stay well below 140 ºC (413 K) which is taken as the maximum bearing temperature, while the inverter temperature sometimes overshoots the 400 K. A safe temperature limit for power electronics is probably around 388 K, based on literature indications for passive components [10]. It should be noted, however, that in these lumped mass calculations the heat transfer from the interior to the surface of components is assumed to be uniform and instantaneous, which is only a coarse approximation of reality.

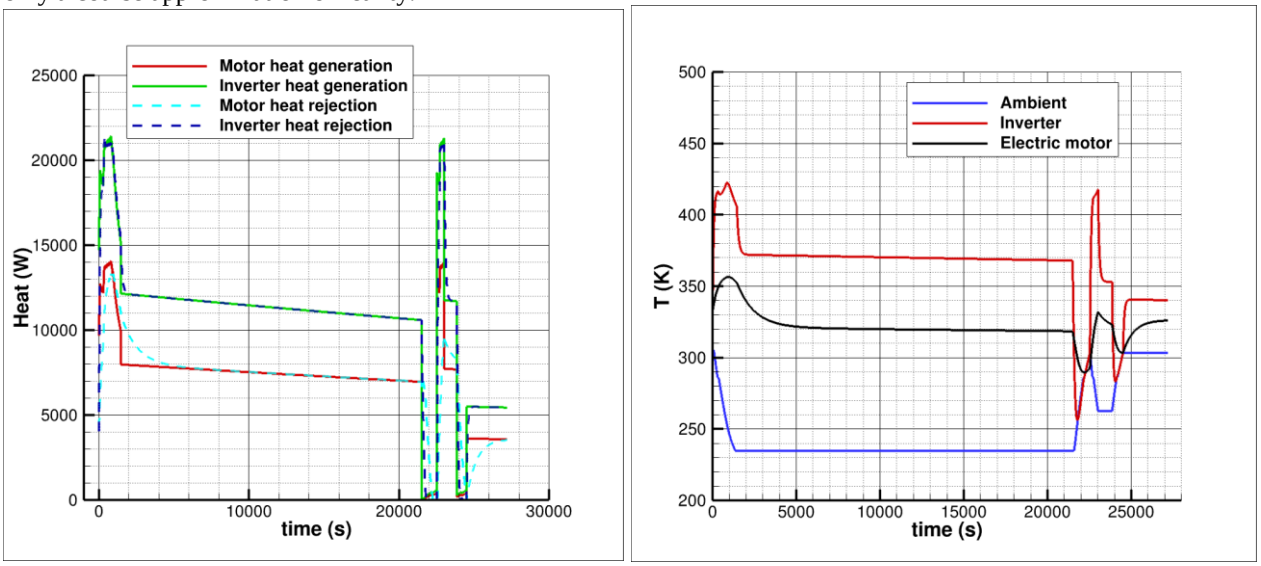

Figure 9: EPU-components heat generation and heat rejection due to convection and radiation (left), and resulting temperature histories (right).

3.3 More advanced compartment model

In our previous paper [5], a very coarse Cartesian block model was presented to explain the ideas for bay modelling of the configuration, intended to derive values with acceptable accuracy for the areas and volumes of compartments to be used for the mutual thermal interaction of components and compartments as well as with the ambient environment. Currently, on the basis of a limited number of main geometrical characteristics, the compartment model has been updated to the real aircraft scale using representative shapes by application of CAD software to deliver a reasonable first impression of the configuration, its bays, and the volumes and interconnecting areas. The latest version of the compartment model is shown in Figure 10. Integration of this compartment model in the TMS is one of the next steps to do.

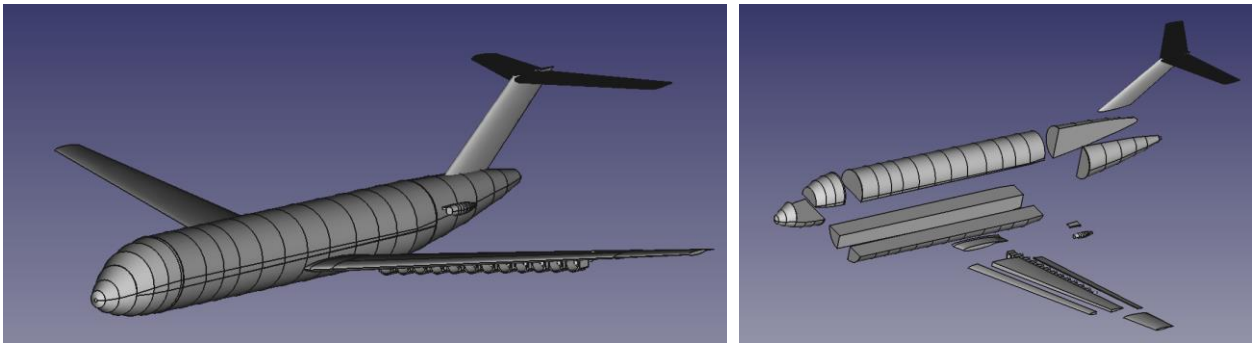

Figure 10: Configuration modelling on the basis of main geometrical characteristics and dimensions (left), showing the compartment split with associated areas and volumes (right)

DOI: 10.13009/EUCASS2023-375

4. Parameter variation impact

4.1 Component efficiencies

The impact of component efficiencies has a direct effect on heat loads and cooling requirements, but also on fuel consumption. State-of-the-art efficiencies used as baseline set, see [5], are reproduced in Table 1, together with a list of projected efficiencies for the year 2035. This list is indicative for now, as a lot of discussion has already been held over the numbers and more discussions will probably lie ahead. Often, discussions on efficiencies are mystified due to deviations in the precise definitions used. One example can be given for the generator. In our previous paper [5], the value of 0.95 has been used as overall generator efficiency. In an initial industrial thermal cooling analysis, this value has been split into a mechanical part (losses in bearings and gears) and an electrical part (losses in the windings) for the sake of attributing the heat loss parts to the correct cooling loop by either the windings coolant or the bearings lubricant oil. The previous overall efficiency value of 0.95 largely complies with the current state-of-the-art split numbers for generator (electric part) and bearings/gears as shown in Table 1.

Table 1: Current state-of-the-art and future projected efficiencies of components

Component	**State-of-the-art efficiencies**	**Projected efficiencies 2035**
Motor (electric part)	0.98	0.99
Inverter	0.98	0.985
Electric bus	0.99	0.99
Cabling	1.00	1.00
Rectifier	0.98	0.985
Generator (electric part)	0.97	0.99
Turboshaft engine	0.46	0.46
Bearings/gears	0.99	0.99

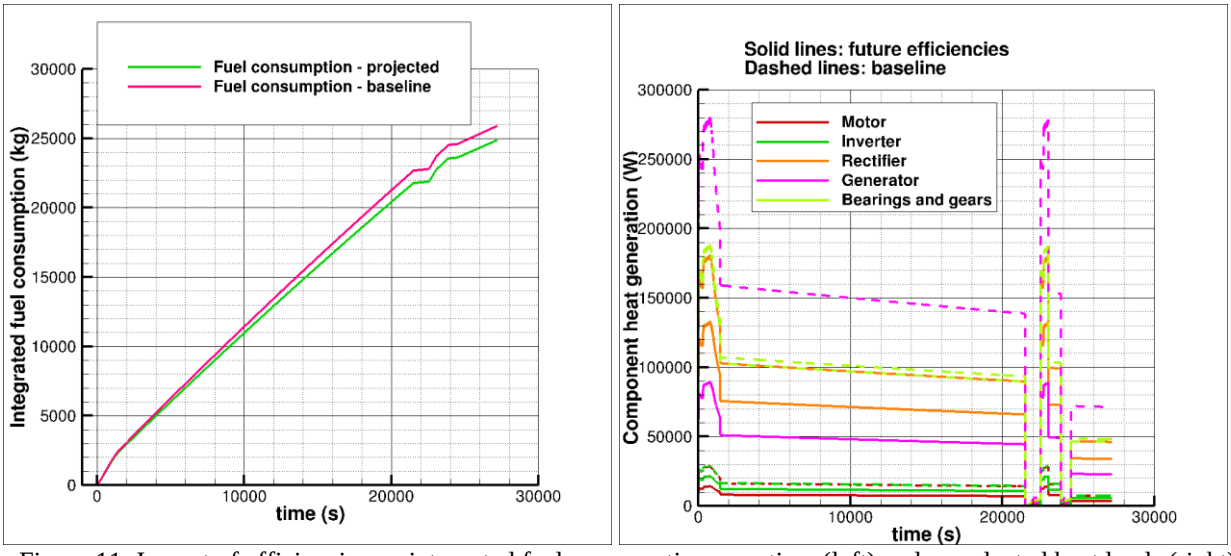

Figure 11: Impact of efficiencies on integrated fuel consumption over time (left) and on selected heat loads (right).

DOI: 10.13009/EUCASS2023-375

The direct implication of changes in efficiencies from baseline state-of-the-art numbers to future projected numbers on fuel consumption is shown in Figure 11 left and on the component heat loads in Figure 11 right. Fuel consumption can be reduced by 4 percent by anticipating higher efficiency components in the drivetrain. The component heat loads (only a selection is shown here, as the buses are not that much different from the baseline situation) are significantly lower for the assumed improved efficiencies, implying that the cooling of those components is posing a lower burden on the TMS. Despite the unchanged efficiency of bearing and gears as well as engine, the bearings and gears heat loads have dropped by about 4 percent due to the combined efficiency improvements in the drivetrain. The indirect effects due to potential aircraft weight reductions due to a lighter TMS have not yet been assessed, as it requires a detailed elaboration of TMS weight estimates and their impact on aircraft level.

4.2 Fuel return loop

Modelling of aircraft fuel tank thermal system has been inspired by [11] and [12]. The fuel return loop is being used in order to be able to extract more heat from the generator coolant. The impact of the fuel enhancement factor λ on coolant and fuel temperature and on the fuel tank temperature is shown in Figure 12. It should be noted that fuel is only being used as a coolant during the high temperature loading take-off and climb phases of the flight profile. This can be seen as the time during which the fuel tank temperature (T_FT in Figure 12) increases. Furthermore, the natural process of cooling of the fuel contained in the tank by convection and radiation to the ambient environment has not yet been included here, so that the fuel tank temperature remains constant during cruise. The fuel enhancement factor λ has been varied between 0 and 4. For zero additional fuel cooling (λ=0), the fuel tank temperature remains at its initial value as no heated fuel is returned to the tank. In this case, all the fuel pumped up by the fuel pump is being combusted. However, the peak loads visible in fuel temperature (T_FOHX1F) and coolant temperature (T_FOHX1C) are high in the take-off and climb phases and the fuel temperature actually exceeds its limiting temperature. For λ=3, the fuel tank temperature rises moderately in take-off and climb and remains constant during cruise as there is no fuel returning to the tank in that phase, but rises much quicker in the diversion climb around approximately 23000 seconds in flight. This is due to the smaller amount of fuel remaining in the fuel tank at the end of the cruise phase. The peaks in fuel and coolant temperature are reduced by the larger amount of fuel being used as coolant. The delay in fuel tank warming due to its buffering characteristics following peak power demand is also visible in Figure 12. Finally, for λ=4, the fuel tank buffers more heat and reduces the peak temperatures even further. At the end of flight, the disadvantage of coupling all mass flows by constant factors to the fuel flow (see the assumptions of section 3.1) becomes evident. When fuel consumption drops significantly, all other mass flows including that of the air flowing through the air-oil heat exchanger, are reduced as well and temperatures rise again which is not fully consistent with aircraft state.
Finally, using the first fuel-oil heat exchanger more efficiently by pumping up more fuel than purely needed for combustion also lowers the heat rejected in the air-oil heat exchanger further down the line. As the coolant temperature entering the air-oil heat exchanger is already lower as a result of the higher cooling in the first fuel-oil heat exchanger, the lower temperature difference with the air reduces the heat rejection potential of the air-oil heat exchanger to the environment. All-in-all, there is a delicate balance to be established between the necessary fuel cooling in high power demand phases of flight (internal heat buffering) and the direct heat rejection potential to the environment.

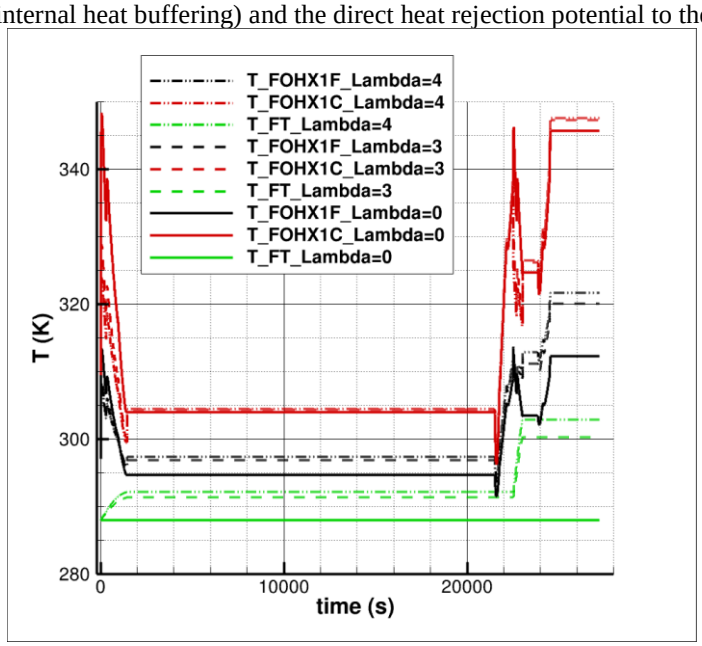

Figure 12: Impact of fuel return-to-tank loop on temperature development of fuel, coolant, and fuel tank temperature.

DOI: 10.13009/EUCASS2023-375

4.3 Bleed air extraction

In the current set-up of the TMS, the amount of air flowing through the air-oil heat exchanger is expected to be either coming from the ram air inlet or, in case of low or absent aircraft speed, from extracted bleed air from the compressor in order to force the cooling air flow. The amount of ram air and its temperature, deduced from the flight profile and assuming an effective capture area of 0.4 m^2, is shown in Figure 13. In an initial industrial assessment of generator cooling, the amount of air during take-off was set to a constant value of 57.8 kg/s during take-off and initial climb, and 30 kg/s during cruise. These values align quite well with the amount of ram air normally obtained. In taxiing, take-off and initial climb phases at low velocity, however, additional bleed air from the compressor is needed to force the air flow through the air-oil heat exchanger in order to maintain a flow of air. In that case, the temperature of the air flowing through the air-oil heat exchanger will also be higher, depending on the mixture of ram air and bleed air. The impact of air temperature on coolant temperature is immediate, as no delays in heat exchangers are modelled. Higher air temperatures imply higher coolant temperatures by the same amount. Higher air flow rates will show up in lower output air temperatures, but not in lower coolant temperatures as the coolant is the determining characteristic fluid of the air-oil heat exchanger. If, however, more coolant is pumped around, the impact on resulting coolant temperature is shown in Figure 14. The coolant temperature is shown to drop when the coolant mass flow rate is increased by 10 and 20 percent, but not in a linear fashion as the other coolant loop system interactions play a role here, e.g. via fuel-oil heat exchanger 1.

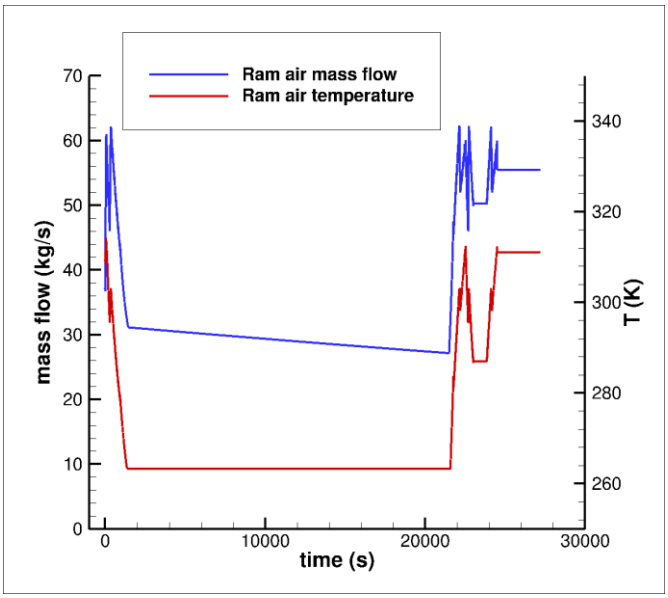

Figure 13: Ram air flowing through the air-oil heat exchanger, derived from the prescribed flight profile.

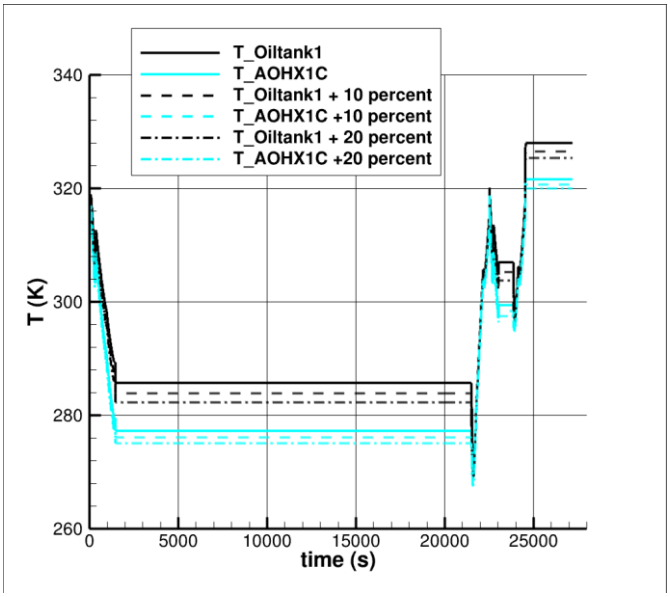

Figure 14: Impact of higher coolant flow rate on coolant temperature from air-oil heat exchanger and in oil tank 1.

DOI: 10.13009/EUCASS2023-375

4.3 Heat exchanger efficiencies

Current values of the heat exchanger efficiencies have been taken over from initial industrial assessments. Supposing that heat exchangers can be upgraded to somewhat higher efficiencies, what would that imply on the resulting oil and coolant temperatures? The parameter variation study for the heat exchanger efficiencies is shown in Figure 15, where the oil and coolant temperatures coming from the heat exchangers are depicted for the initial as well as for 5 and 10 percent higher efficiencies. The largest impact of a higher heat exchanger efficiency is observed in the second fuel-oil heat exchanger, cooling the engine and generator bearings and gears oil. Here, a 10 percent higher heat exchanger efficiency implies a 9 degrees lower oil temperature. For the first fuel-oil heat exchanger and for the air-oil heat exchanger, there is also an impact on oil and coolant temperature but of a smaller order, within just a few degrees. All in all, the efficiencies of heat exchangers do not appear to be very critical parameters on overall system performance, but it may make a difference in the weight of the heat exchangers of the TMS.

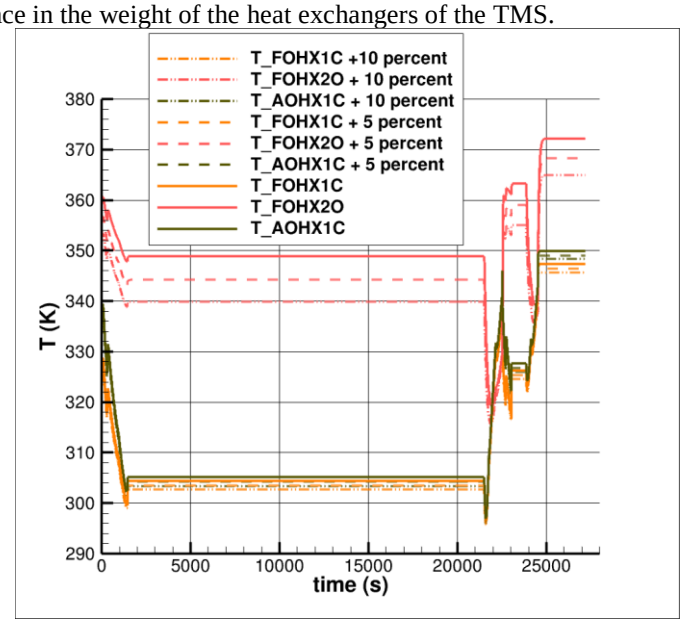

Figure 15: Oil and coolant temperatures coming out of the heat exchangers resulting from a parameter study of heat exchanger efficiencies using 5 and 10 percent higher than baseline values.

4.4 EPU cooling area enlargement

In view of the current lumped cooling calculations of the motor and inverter using airflow over the hub area as heat sink, optimistic values may have been obtained for the heat transfer from the smooth surface of the hub. This is due to the assumption of uniform temperatures that are inherent to lumped modelling. Nevertheless, with the heat transfer coefficient values currently used it appears to be possible to keep the motor and inverter quite well within the desired temperature range. Some more in-depth analysis would be needed to qualify the reality of the heat transfer coefficients. In any case, by using fins, the cooling of motor and inverter can be improved over the default smooth casing situation. Within the IMOTHEP project, effort has been devoted to the numerical assessment of convective cooling capacity increase due to the addition of square-shaped fins on the surface of the motor and inverter housing (effective cooling area enlargement), so that background data are available for either 20 or 60 rows of fins circumferentially. The fin height has been varied using the values of 0.05, 0.10, or 0.20 m height. In each row, the length of fins and interruptions between fins are equal to the height of the fins. Translated into total cooling surface, this comes down to a factor between about 2.3 to almost 17 times the original smooth surface area, indicating that fins can potentially make a large difference. However, fin efficiency needs to be considered here. Fin efficiency is defined as the ratio of actual heat flow to that which would be obtained with a fin of constant temperature uniformly equal to the base surface temperature, that is, one with infinite thermal conductivity. Numerical simulations have shown that the effectiveness of the fin height variations already reach an asymptotic optimum for a height of 0.1 m. Such fins are indeed quite high compared to the original hub diameter. In our current analysis, assuming fins with heights of 0.05 m and 20 rows of fins circumferentially would increase the total convective and radiative area to an equivalent hub diameter of 0.558 m, assuming a fin effectiveness of almost unity. Taking this value in an additional calculation, the impact is visualized in Figure 16. A significant temperature decrease is shown over the entire flight profile, shaving off peaks of the temperatures. Although the area increase in combination with uniform temperature of the lumped modelling of the EPU may give an overly optimistic view on cooling of the EPU, the expectation is that parameter values of fin height

DOI: 10.13009/EUCASS2023-375

and amount of circumferential rows of fins can be optimized in order to meet the cooling requirements. Therefore, a strict necessity of liquid cooling appears to be ruled out by the current analysis.
Despite the focus on air cooling of the motor and inverter in this section, discussions within IMOTHEP regarding the potential of liquid motor cooling options have not yet been settled. Liquid cooling would increase the specific power and the power density of the EPU significantly, however at the cost of a more complex TMS.

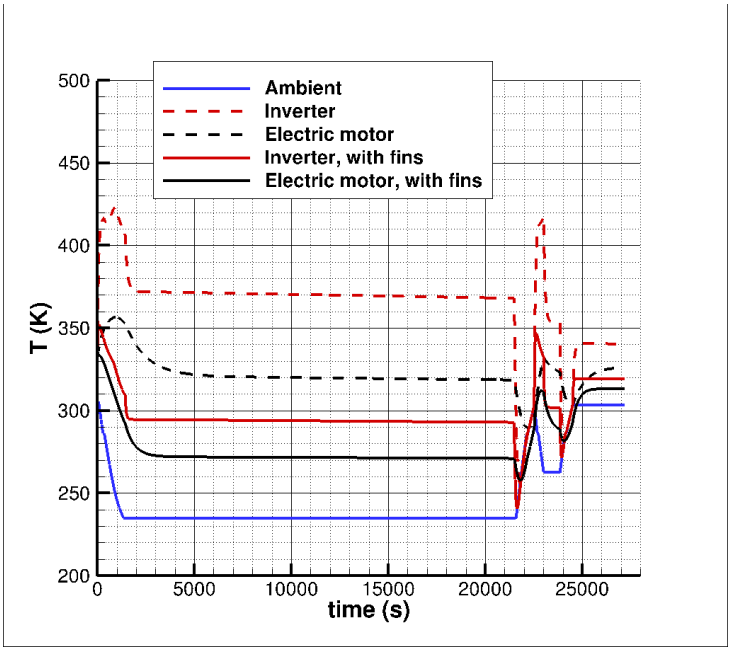

Figure 16: Impact of fins (20 rows circumferentially, 0.05 m height) on resulting temperature of motor and inverter.

4.4 Initial pathway to TMS weight and volume considerations

Heat exchanger weight and volume are determining factors on the resulting overall aircraft level impact of the TMS. Additional components like pumps, tanks, fans, tubing and ram air channels also enter the picture; these can be estimated, obtained or derived from existing equivalent flying configurations if such data are known. For the heat exchangers, an initial estimate can be based on the heat exchanger theory of effectiveness versus the number of transfer units (NTU). For counterflow heat exchangers, the theoretical relation between effectiveness and NTU is depicted in Figure 17.

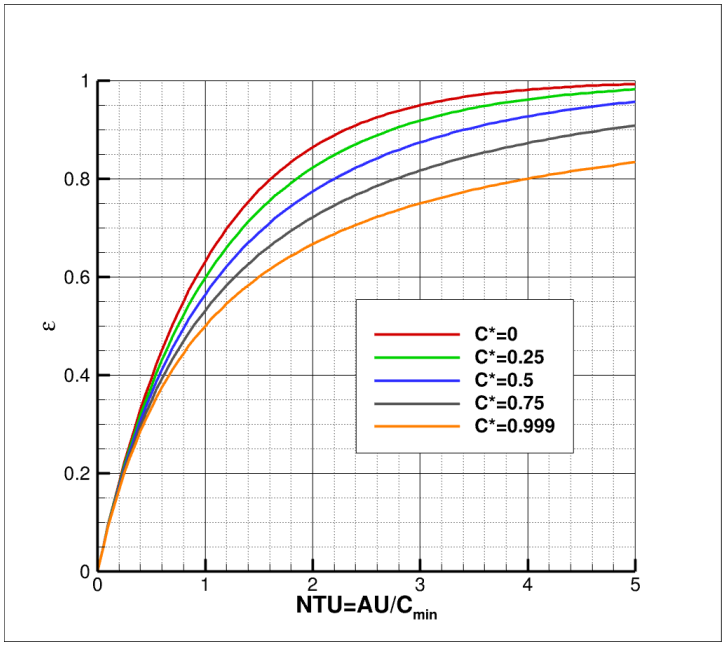

Figure 17: Counterflow heat exchanger effectiveness as function of ratio of heat capacities C^* and NTUs

DOI: 10.13009/EUCASS2023-375

As shown, the curve may differ depending on the ratio of $C^* = C_{min}/C_{max}$, which is the heat capacity ratio of both fluids. In designing a heat exchanger, some iteration or experience will be required to define the number of NTUs and the resulting efficiency against a suitable flow rate of both coolants. Such processes are more detailed in e.g. [13]. Once the iteration on effectiveness and NTU has been settled, the heat exchanger area A times the heat transfer coefficient U is known from NTU and C_{min}. With a realistic estimate of the heat transfer coefficient, the required area is known. Using heat exchanger compactness ratio indications such as given by [13] and [9] for compact heat exchangers, a value for the volume of the heat exchanger is obtained. Similarly, the mass of the heat exchanger can be calculated when a material choice has been done, using the material density. For the mass calculation, also the porosity factor of the heat exchanger needs to be known, i.e. the internal set-up of the heat exchanger in terms of tubing and dimensions. The porosity factor is a factor in the interval between 0 and 1 (zero meaning no porosity and thus no flow at all possible; one meaning fully open and no heat exchanger mass remaining). However, the task of determining a sensible set of realistic heat exchanger parameters should not be underestimated. Further elaboration is needed in order to come up with useful weight and volume estimates according to the sketched pathway.

5. Concluding remarks and way forward

A framework for the analysis of aircraft level heat production and requirements of cooling loops over a typical flight profile has been established. Due to the lumped nature of modelling requiring a minimum of input data, the methodology can be applied with equal ease to existing aircraft as well as to preliminary designs of new concepts. Integration and interaction of cooling loops have been established and verified. By addition to or adjustments of the underlying architecture, many types of aircraft can be handled in this way. Parameter studies can be performed in order to visualize trends, find limitations of specific architectures, or establish a better vision on cooling requirements. Enhancement of the lumped approach using more detailed analysis results from specific component studies is in all cases possible by inclusion of more accurate heat transfer coefficients and surface temperature information.

A specific hybrid-electric architecture for a conservative tube-and-wing SMR configuration has been studied. The anticipated cooling loops for electrical generator cooling and EPU cooling have been studied in detail. These cooling loops include the use of air for the EPU, but also liquid coolants and even fuel to control the high heat loss peaks for the generator during high power-demand flight phases. Despite some missing details in the modelling that need further elaboration, the main trends obtained from the architectural modelling are found to be consistent. Air cooling for the EPU is expected to be sufficient at the powers considered by optimizing heat transfer to the fan-induced air flow through the ducts. For the interaction between the liquid coolant loops, further optimization can be studied in terms of parameter variations on the amounts of liquid coolants to be pumped around, and the optimal heat rejection to ambient air.

An initial pathway for calculating heat exchanger volume and weight has been outlined. The task of determining a consistent set of realistic heat exchanger parameters, however, is not straightforward and requires some further elaboration and validation before useful weight and volume estimates can be obtained for the heat exchangers. Further integration with the foreseen compartment model to add mutual heat exchanges between bays and with the ambient environment through airframe walls is the next step to be performed.

Acknowledgment

The reported work has been performed within the framework of the IMOTHEP project [6]. The authors acknowledge the valuable discussions with and contributions obtained from IMOTHEP partners to this work as well as the funding received from the European Union's Horizon 2020 research and innovation programme under grant agreement No. 875006.

References

[1] Paris agreement to the United Nations framework convention on climate change", Dec. 12, 2015, T.I.A.S. No. 16-1104.

[2] J.H. Kim, K.S. Kwon, S. Roy, E. Garcia, and D. Mavris, 2018. Megawatt-class turboelectric distributed propulsion, power, and thermal systems for aircraft. *AIAA paper 2018-2024*.

[3] R. Larkens, 2020. A coupled propulsion and thermal management system for hybrid electric aircraft design – a case study. *MSc. Thesis, Technical University of Delft*.

[4] P. Abolmoali, A. Donovan, S.S. Patnaik, P. McCarthy, D. Dierker, N.Jones, and R. Buettner, 2020. Integrated propulsive and thermal management system design for optimal hybrid electric aircraft performance. *AIAA paper 2020-3557*.

DOI: 10.13009/EUCASS2023-375

[5] J. van Muijden and V.J.E. Aalbers, 2022. Thermal management principal analysis of hybrid-electric aircraft with turboelectric propulsion using distributed propulsors. *Paper presented at 9th European Conference for Aeronautics and Space Sciences (EUCASS)*, 28 June – 1 July 2022, Lille, France.

[6] www.imothep-project.eu

[7] Ph. Novelli, S. Defoort, N. Tantot, D. Zimmer, D. Varchetta, Ch. Viguier, and P. Iodice, 2023. IMOTHEP European project: an investigation of hybrid electric propulsion for commercial aircraft. *Paper presented at the AIAA Aviation Forum*, 12-16 June 2023, San Diego, CA.

[8] https://www.onera.fr/en/news/how-can-we-reduce-fuel-consumption%3F-dragon

[9] J.P. Holman, 1986. Heat transfer. 6th Edition, McGraw-Hill.

[10] J. Biela, M. Schweizer, S. Waffler, and J.W. Kolar, 2011. SiC versus Si – Evaluation of potentials for performance improvement of inverter and DC-DC converter systems by SiC power semiconductors. *IEEE Transactions on Industrial Electronics*, Vol. 58, Issue 7, pp. 2872-2882.

[11] B.J. German, 2011. A tank heating model for aircraft fuel thermal systems with recirculation. *AIAA paper 2011-641*.

[12] R. Manna, N. Ravikumar, S. Harrison, and K.Goni Boulama, 2021. Aircraft fuel thermal management system and flight thermal endurance. *Transactions of the Canadian Society for Mechanical Engineering*, TCSME-2021-0146.

[13] W.M. Kays and A.L. London, 2018. Compact heat exchangers. 3rd Edition, MedTech.